ELSEVIER

Journal of Physics and Chemistry of Solids 64 (2003) 299–306

JOURNAL OF PHYSICS AND CHEMISTRY OF SOLIDS

www.elsevier.com/locate/jpcs

Electrical and chemical characteristics of nano-meter gold encapsulated in mesoporous and microporous channels and cages of FSM-16 and Y zeolites

Mohamed Mokhtar Mohamed[a,*], Ibrahim Mekkawy[b]

[a]*Department of Chemistry, Faculty of Science, Benha University, Benha, Egypt*
[b]*Department of Physics, Faculty of Science, Al-Azhar University, Assiut branch, Assiut, Egypt*

Abstract

The dc and ac conductivities as well as the dielectric constant (ε') were measured for different zeolites encapsulated gold ($AuCl_3$) samples at different temperatures (300–500 K) and various frequencies (5 kHz–1 MHz). The conductivity was found to change in the order Au/FSM-27 > Au/NaY > Au/FSM-47. Sorbed water contained inside zeolites assists greatly the proton mobility (zeolite protons) and the ion mobility (Na^+ and Au^+) and hence enhance the electric conduction in the temperature range 300–373 K. Raising the temperature over 373 K induces dehydration effect that assists the metallic gold formation and thus a dramatic loss in conductivity was revealed. The conduction mechanism was expected to be partially ionic and partially electronic. The IR study showed that the exposure of Au zeolites to CO gas produced a characteristic band of Au^+–CO at 2180 cm^{-1} that tends to decrease with temperatures and even vanishes at 376 K in favor of Au^0–CO at 2128 cm^{-1}. Similarly, a phase transition at 338 K, that occurs in the range 300–376 K, was confirmed by DTA to further emphasize the temperature regions of either Au^+ cations (338 K) or Au^0 (376 K) formation.

Keywords: NaY; FSM-16; Gold; CO adsorption; DTA; D. Electrical properties

1. Introduction

Electrical properties of dielectrics and semiconductors are of great interest because of their wide use in modern electronic devices [1–6]. The electrical properties of these materials depend not only on the chemical composition and structural features but also on the preparation conditions [7,8]. On the other hand, dielectric investigations provide a fundamental way for studying the rotation of dipoles and hopping of electrons involved in the conduction process [9].

Recently, gold has attracted the high attention as a catalyst or sensor especially when it's encapsulated inside zeolites. Major research in intrazeolitic gold catalysts explored high catalytic activities towards some reactions such as water gas shift reaction and NO reduction by CO in presence and absence of hydrogen [10–12]. This was due to high degree of dispersion of Au^+ species inside zeolites. It has been reported that Au incorporated inside zeolites by means of a chemical vapor deposition (CVD) method resulted in a controlled particles size of gold species in the range 3–20 nm [13]. Accordingly, the particular interest nowadays in nano-technology; in view of utilizing it in different areas such as semiconductors, chem-bio-engineering and sensors, encouraged us to study the chemical and electrical properties of $AuCl_3$ when encapsulated inside the microporous NaY zeolite or inside mesoporous materials such as FSM-16. The latter material, which have honey comb structures with ordered enormous channels of 20–100 Å diameter attracted current interests because of its potential host for the inclusion of large organic or inorganic molecules [14]. The encountered accessibility of FSM-16 to large substrates over microporous cavities (6–13 Å), of conventional zeolites such as NaY, opened up new applications in catalysis [15].

2. Experimental

2.1. Materials preparation

Linde zeolite NaY (LZY, Lot No. 030785) was used as a

* Corresponding author. Tel./fax: +20-13-222-578.
E-mail address: mohmok2000@yahoo.com (M.M. Mohamed).

0022-3697/03/$ - see front matter © 2002 Elsevier Science Ltd. All rights reserved.
PII: S0022-3697(02)00300-1

Table 1
Some physical properties of the employed zeolites

Zeolite type	Si/Al ratio	Surface area ($m^2\ g^{-1}$)	Pore size (Å) and (its structure)
FSM-16 (mesoporous)			
FSM-27	300	950	27 (channels)
FSM-47	300	670	47 (channels)
NaY (microporous)	5.6	850	7.5 (cages)

starting material. According to the published procedures [16] the host FSM-16 was synthesized using a layered polysilicate (Kanemite; $NaHSi_2O_5$: $3H_2O$) and $C_{16}H_{33}NMe_3Cl$ as a micelle surfactant template, similar to MCM-41 [17]. After calcination at 823 K, the resulting material (surface area, 950 m^2/g) presents well-defined hexagonal mesoporous channels with silanol groups (3745 cm^{-1}), which were identified by X-ray powder patterns and TEM techniques [18]. Variation of channels diameter depend on the surfactant chain length. FSM-27 and FSM-47 will be used to describe materials with the FSM-16 structure of pore sizes 27 and 47 Å, respectively.

The 2.5 wt% Au/NaY, 2.5 wt% Au/FSM-27 and 2.5 wt% Au/FSM-47 samples were prepared at room temperature by careful mechanical mixing of $AuCl_3$ (strem chemicals, 99% purity) with NaY, FSM-27 and FSM-47 zeolites under a nitrogen atmosphere. The samples were subjected to heat treatment at 338 K for 48 h under a reduced pressure of 10^{-6} Torr. The temperature was increased at a rate 0.2 K min^{-1} from room temperature to 338 K. This temperature was sufficient for an effective sublimation of $AuCl_3$ [10–13]. The $AuCl_3$ solid was slowly vaporized and migrated to interact with water molecules in the zeolites pores or channels [11]. Some physical properties of the employed zeolites were presented in Table 1.

2.2. Techniques

2.2.1. FTIR investigation

Infrared spectra of CO adsorbed at room temperature on various investigated samples were recorded with a Jasco double beam FTIR-5300 spectrometer with 40 co-added scans at 4 cm^{-1} resolution. Each sample was pressed into a self-supporting wafer and mounted in a quartz infrared cell and subjected to heating at 323 K under a reduced pressure of 10^{-4} Torr prior to the CO adsorption.

2.2.2. Thermal analysis

TG and DTA analyses were conducted for different uncalcined Au-zeolite samples using automatically recorded model 50 Shimadzu unit. The rate of heating was fixed at 10 K min^{-1} and the heating process was done in a flow of dry air at a rate of 40 cm^3 min^{-1} from room temperature up to 873 K.

2.2.3. X-ray diffraction (XRD)

The X-ray patterns for Au-encapsulated zeolite samples were collected on a Diano automated powder diffractometer by using Co Kα radiation.

2.2.4. Conductivity measurements

The electrical measurements were carried out on different solid samples in the form of pellets (10 mm diameter and 0.5 mm thickness) subjected to hydraulic pressure of 5.0×10^3 kg cm^{-2}. The dc and ac electrical conductivity measurements as well as the dielectric constant were carried out using the two-probe method. The pellets were tightly interfaced with polished silver disks in the Cu electrode holder. The ac conductivity (σ_{ac}) and the dielectric constant (ε) were measured at different temperatures (300–500 K) as a function of the applied frequency (5 kHz–1 MHz) using Hioki bridge type 3530 (Japan). The dc conductivity was measured using Keithly electrometer type 416 (USA). A T-type thermocouple was inserted just to exert smooth contact with the sample, to measure the temperature and, to avoid any temperature gradient. The accuracy of the measured temperature was better than ± 1 K.

3. Results and discussion

Fig. 1 shows the dc conductivity curves ($\ln \sigma_{dc}$ vs. reciprocal of absolute temperature) for different zeolite samples encapsulated gold samples. Inspection of Fig. 1 revealed that: (i) The electrical conductivity of different investigated Au treated zeolites increases by increasing the temperature reaching to a maximum limit at 373 K and decreases upon increasing the temperature above this limit. (ii) The electrical conductivity depends on the nature of the employed zeolite, it decreases in the following order Au-FSM-27 ≥ Au/NaY > Au-FSM-47. These results clearly indicate the semiconducting behavior of different investigated samples at temperatures reaching 373 K. Above this temperature they exhibit a metallic conduction. The conductivity of a given solid is a function of charge carriers concentration (n) × their mobilities (μ). So, Au/FSM-27 showed the maximum $n\mu$ values and Au-FSM-47 showed the lowest $n\mu$ values. The charge carriers in the investigated materials has previously been demonstrated [19] to be H^+

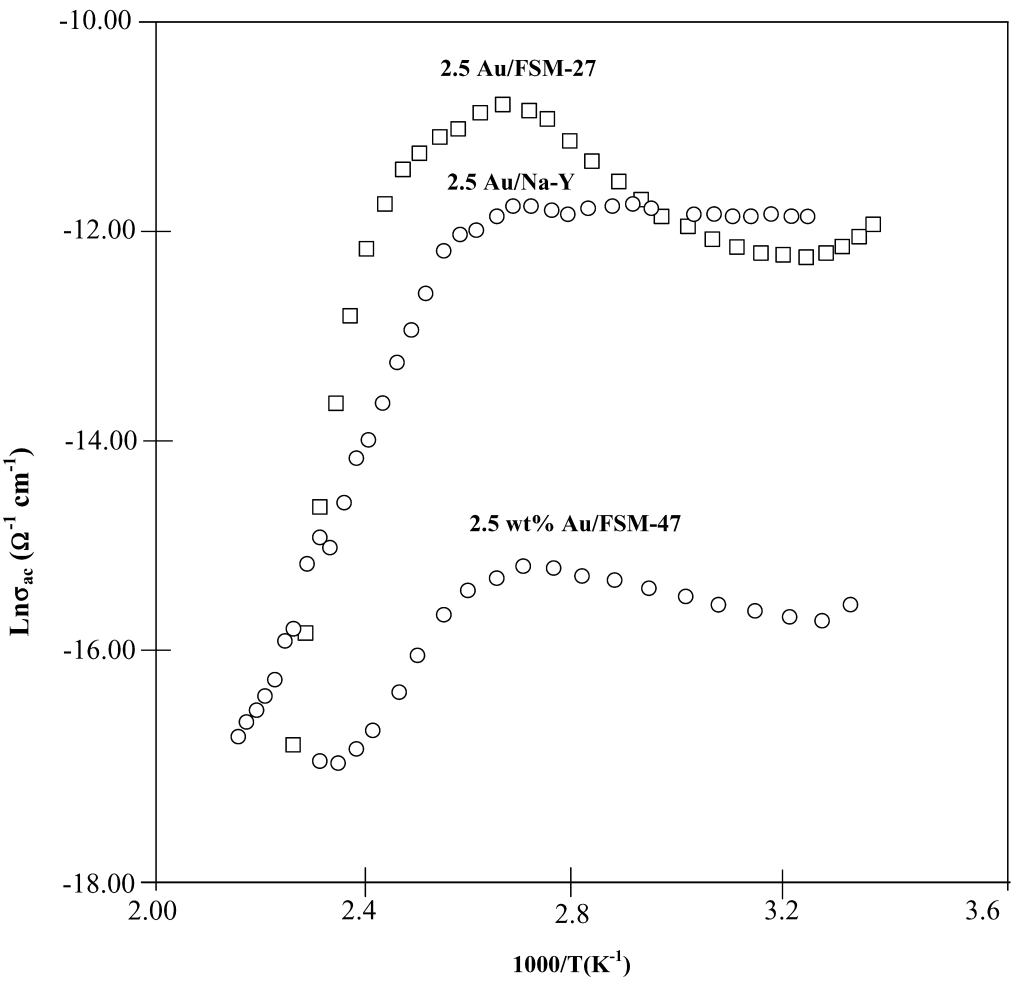

Fig. 1. Dependence of dc conductivity on inverse temperature for 2.5 wt% Au/FSM-27, 2.5 wt% Au/NaY and 2.5 wt% Au/FSM47 samples.

and Au^+ as well as Na^+ ions. The concentration of Au^+ ions can be much affected by the degree of dispersion of Au species present. The mobility of charge carriers might be affected by geometrical parameters of zeolites, e.g. its pore diameter. The bigger the pore size the easier the diffusion of charge carriers and the higher the mobility. It can be seen from Table 1 that FSM-27 zeolite exhibited the biggest surface area (950 $m^2\,g^{-1}$) and should led to a maximum degree of dispersion of Au^+ ions, i.e. maximum concentration of one of charge carriers. So, the maximum conductivity of Au-FSM-27 could be understood. On the other hand, Au-FSM-47 showed minimum electrical conductivity and minimum $n\mu$ values due to the minimum degree of dispersion of Au ions. This effect might result from its smallest specific surface area (Table 1). Au/NaY zeolite, the most rich in protons concentration might be expected to have a relatively high value of electrical conductivity. This speculation has not been verified experimentally. This could be due to either the limited contribution of hydrogen protons to electrical conduction or to the decrease in the mean free path inside NaY cages as a result of increasing the number of charge carriers (Au^+, H^+ and Na^+).

The X-ray diffraction patterns of the Au-FSM-27 and Au-FSM-47 samples are shown in Fig. 2. The samples exhibited the same crystalline pattern of the parent FSM-16 sample that used to have intense reflections at $d = 37.33$ and 22.26 Å. No lines due to the $AuCl_3$ crystalline phase ($2\theta = 18.7$, 20.5 and 22.26° for Co Kα) appeared after heat treatment at 338 K for both samples. This implies that $AuCl_3$ is highly dispersed and probably is located in the internal surface of zeolite similar to what has been reported formerly on $AuCl_3$/NaY [20]. From the XRD patterns, the Au metallic phase at $2\theta = 44.71$ and 52.09° was observed for both samples where a greater intensity in the Au-FSM-47 pattern was obtained. The estimated dispersion of Au particles (20 nm) inside FSM-27 channels was considerably higher than that in FSM-47 channels (50 nm), as has been validated by XRD measurements using Scherrer equation.

The transformation of charged Au in zeolites may take

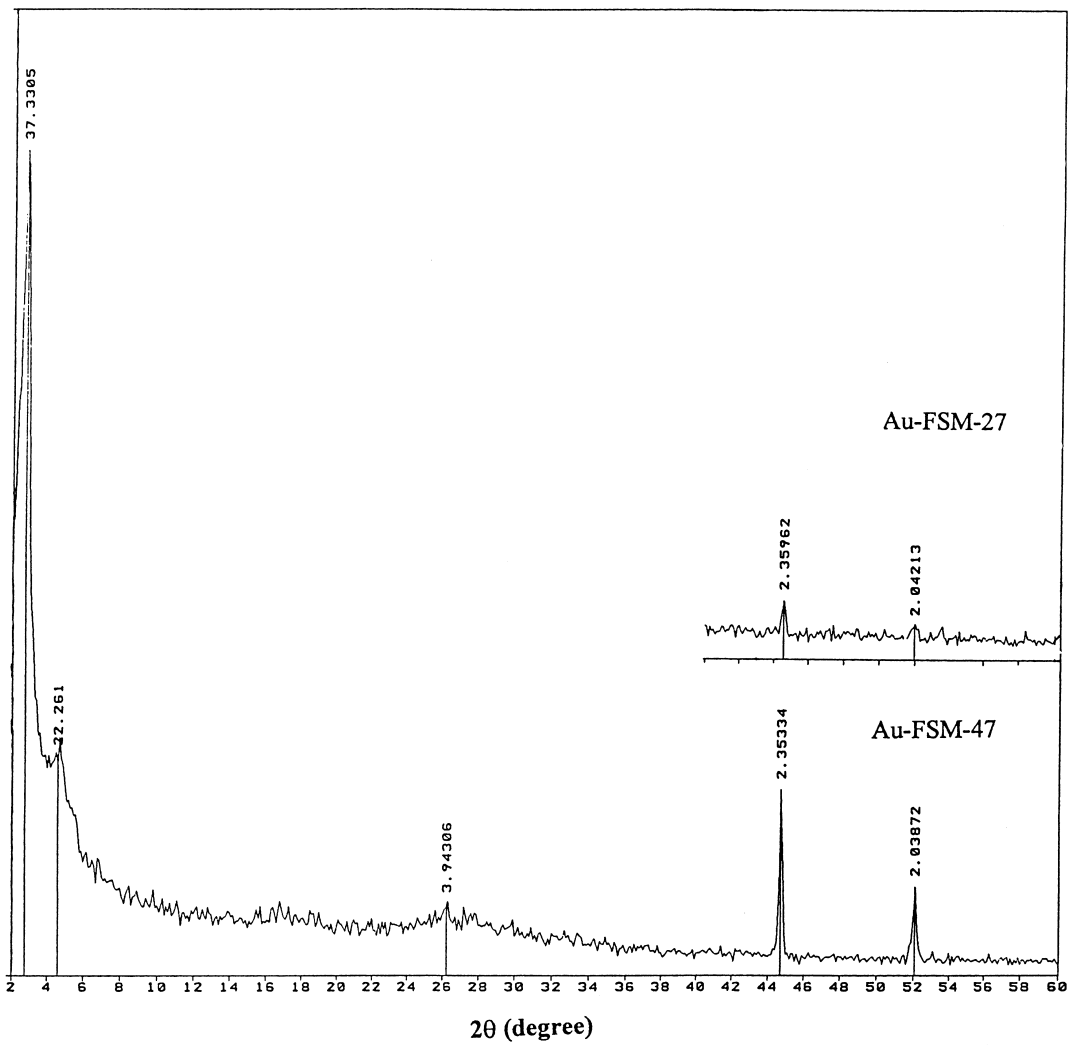

Fig. 2. XRD diffraction patterns of 2.5 wt% Au-FSM-27 and 2.5 wt% Au-FSM-47 samples treated at 338 K.

place according to the following reaction [11]:

$$3Au^{+} \rightarrow 2Au^{0} + Au^{3+}$$

It has been reported that Au^{+} is metastable and slowly disproportionates to Au^{3+} and Au^{0} [19] as can be seen in the former equation. However, this disproportionation is not significant in the case of NaY because of the strong interaction of $AuCl_n$ with NaY zeolite [19,20]. Conversely, in the case of FSM-27 the interaction of $AuCl_n$ is expected to be of lower strength. Accordingly, electronic conduction can take effect in the conduction mechanism especially in the FSM-27 sample.

Fig. 3 shows the ac conductivity curves ($\ln \sigma_{ac}$ vs. reciprocal of absolute temperature) of the $AuCl_3$/FSM-47 sample at different frequencies. The temperature-dependent σ_{ac} varies significantly with frequency revealing three different straight lines in three different temperature regions. The first region was from 300 to 338 K, in which the conductivity increases with increasing temperature. This may be due to either thermally activated mobility of charge carriers or thermally activated number of the same carrier, or due to the collaboration of the two processes with each other. The second region was from 338 to 417 K where the conductivity was slightly decreased. This was due to the production of metallic gold atoms according to the earlier equation and thus reduces the charge carrier concentration or due to the presence of delocalized zones [21]. σ_{ac} has to rise exponentially with temperature if it depends only on thermal activation. Thus, the earlier drop in σ_{ac} with temperature is then a consequence of the earlier loss in the role of sorbed water assisting the ionic conductivity [22]. In the high temperature region, from 417 to 500 K, the conductivity was dramatically decreased due to the increase in the charge carrier density of Au^{0} and as a result an expected increase in collision can be accomplished causing a decrease in the mobility. With respect to the frequency, it

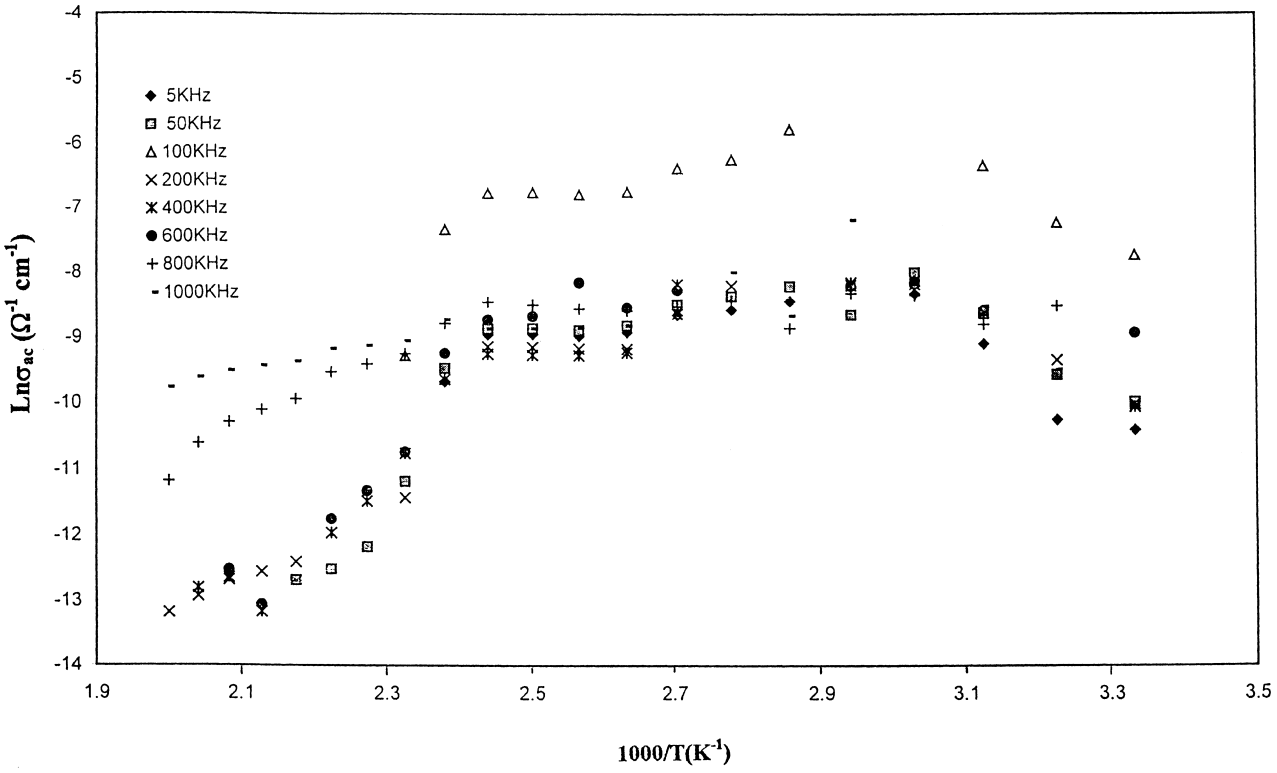

Fig. 3. Dependence of ac conductivity on inverse temperature for the 2.5 wt% Au/FSM47 sample at different frequencies.

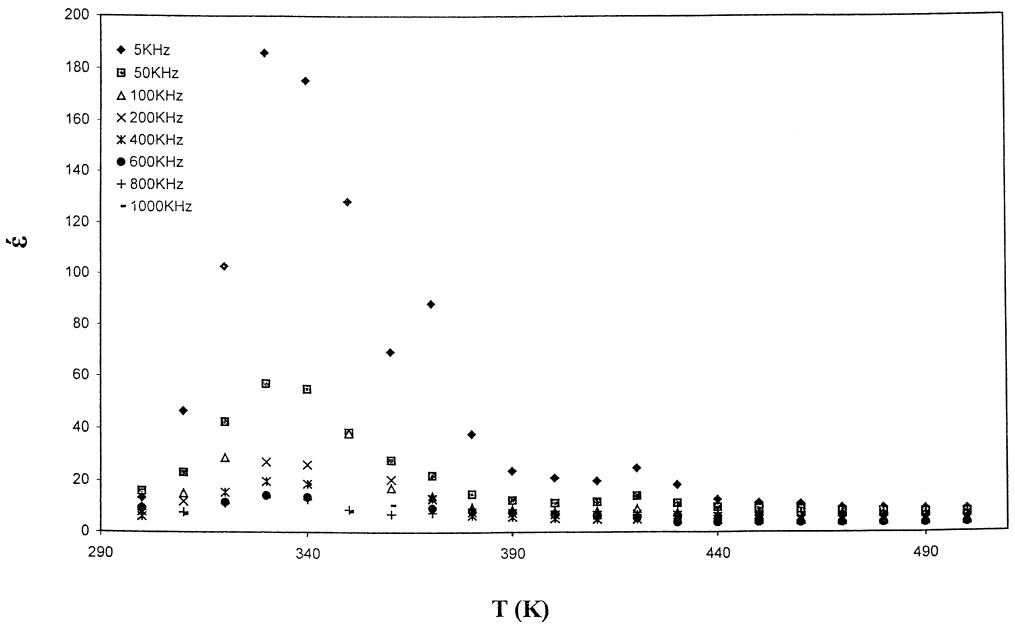

Fig. 4. Dielectric constant for the 2.5 wt% Au/FSM-47 sample as a function of temperature and at different frequencies.

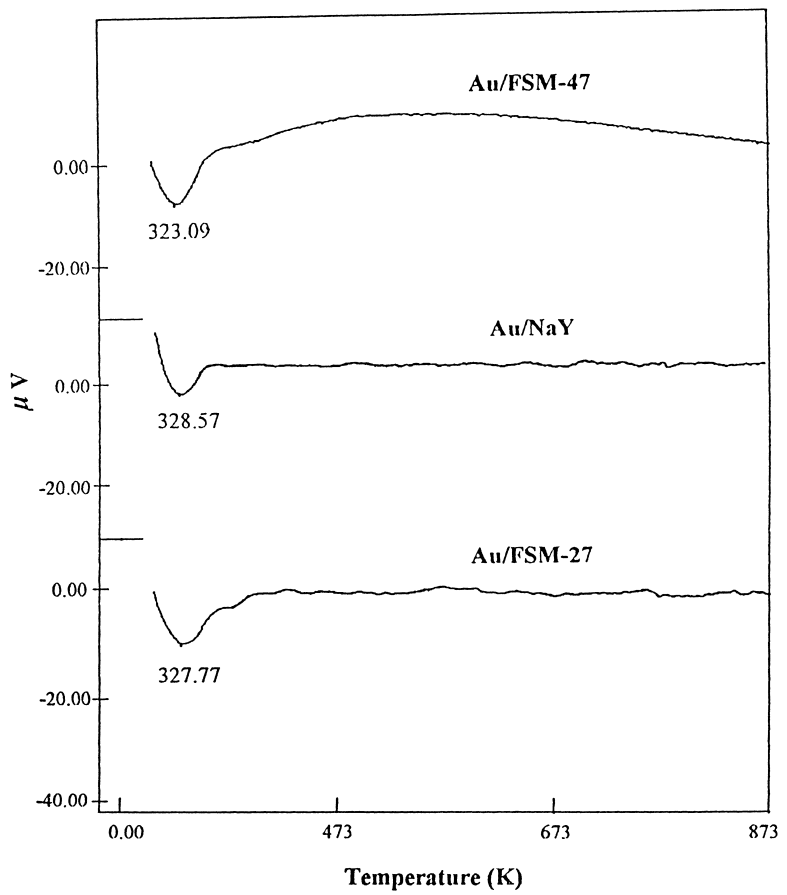

Fig. 5. DTA curves of 2.5 wt% Au/FSM-27, 2.5 wt% Au/NaY and 2.5 wt% Au/FSM-47.

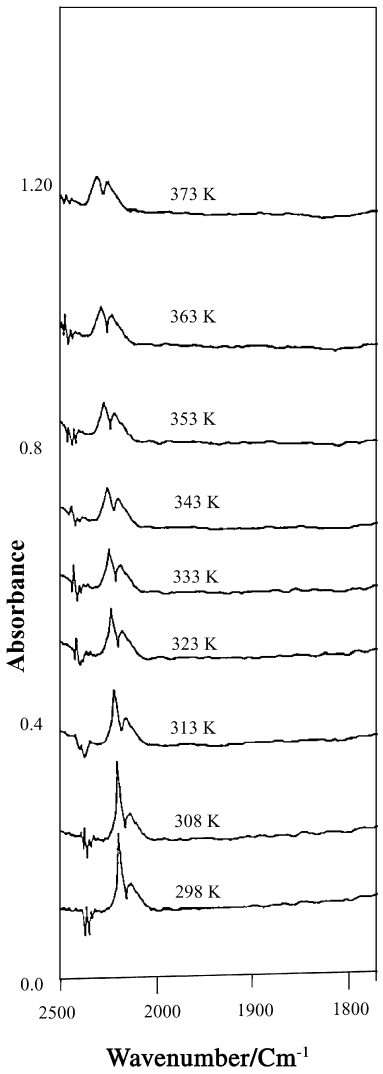

Fig. 6. In situ FTIR spectra of CO adsorption at room temperature on the 2.5 wt% Au/FSM-47 sample as a function of increasing temperature.

is clear that increasing the frequency from 5 to 100 kHz causes promotional effects on the activation energy from 0.5 to 1.3 eV, respectively, in the first range of temperatures (300–338 K). This means that the frequency acts as a disturbing factor affecting aligned dipoles in the field direction, i.e. the charge carriers cannot follow up the field variation accompanying the applied frequency.

The temperature-dependent ε' decreases sharply on raising the frequency to high values beyond 5 kHz (Fig. 4). This increase in ε' showed a maximum around 330 K that coincided with that obtained from DTA thermograms in the range 323–328 K (Fig. 5). In conformity, the weight loss in TGA curve for the FSM-47 sample (not shown) was equivalent to that of Au/FSM-47, implying that the desorption of water, that maintained at 373–385 K, contained inside channels was responsible for the weight loss in TG curves and not Au moieties. Thus, phase transition either in FSM or Y zeolites (Fig. 5) was due to the vital role-played by water on the reduction of Au^{3+} into Au^{+}. This assignment has been supported by XPS data in previous works [19,20].

It seems that water contained inside either channels or cages of zeolites played a unique role not only in provoking the ionic conductivity but also the metallic behavior. This was due to sorbed water may be regarded as a vehicle to carry the protonic charge carriers across silanols over the entire zeolite structure [23]. Accordingly, the zeolite water particularly at the first data points covering the range 373–384 K (Fig. 1) helps the ionic as well as protonic conductivities, which started to lose the supporting role of sorbed water upon raising the temperature range 384–416 K. The former range reflects the earlier role of sorbed water in enhancing the ion mobility and hence the ionic conduction that drops with dehydration, in the latter range, due to the evolution of Au^{0} species. These species were formed upon increasing the temperatures above the boiling point of water, i.e. depletion of water was responsible for the reduction of Au^{+} into Au^{0}. Accordingly, the reaction of $AuCl_3$, vaporized upon heating and diffused inside the zeolite channels, with H_2O occurred as $AuCl_3 + 2H_2O–Z \rightarrow AuCl/Z + 2HCl + 2OH/Z$, where Z refers to zeolite in general [11,19,20]. The evolution of gaseous HCl was monitored by temperature programmed reduction technique [19], as an indication of the interaction of $AuCl_3$ with H_2O contained in the zeolite sample. It has been concluded previously [19] that $AuCl_n$ species did not react with silanol protons in SiOHAl structure; of weak acidity, but rather polarized H_2O in zeolite and promoted the creation of new OH groups during an FTIR study of OH absorption bands of NaY before and after $AuCl_3$ loading.

After the phase transition (Fig. 4), ε' decreases sharply up to 390 K indicating a rapid loss of sorbed water content. In the first data points covering the range 290–330 K, the increase in dielectric constant was due to the increase in polarizability. It can be seen that the small thermal energy was quiet sufficient to liberate some of the localized dipoles, and the field accompanied with the applied frequency orient them in its direction. The outcome of this process is the increase in ε'. After the phase transition, the increase in thermal energy causes an increase in the lattice scattering of the charge carriers. This produces a decrease in the mobility and polarizability. It can be seen that ε' decreases with increasing frequency, which is the general trend of dielectric materials. This is due to that dipoles cannot follow up the field variation (Fig. 4). The same behavior was obtained for Au/NaY and Au/FSM-27 samples (not shown).

Fig. 6 shows the IR spectra in the region 3000–1800 cm^{-1} obtained when an Au/FSM-47 catalyst is exposed to CO adsorption, at room temperature, as a function of increasing temperature. The initial spectrum showed a strong band at 2180 cm^{-1} and a small band at

2128 cm^{-1}. These bands are assigned to the chemisorbed CO onto Au^{+}/FSM-47 and Au^{0}/FSM-47, respectively, as they coincide with those reported for CO-coordinated Au-NaY [11]. It can be seen that the 2180 cm^{-1} band was considerably diminished after raising the temperature to 323 K, indicating a substantial decrease in the Au^{+}–CO species. Thus, an observed decrease in the relative intensity of Au^{+}–CO/Au^{0}–CO with temperature was obtained.

4. Conclusions

The water contained inside Y and FSM-16 zeolites is conceivably responsible for the evolution of charged Au^{+} species that showed a high electrical conductivity in the temperature range 325–373 K. However, a marked drop in the conductivity was evident at high temperatures (>373 K) due to water desorption, which was responsible for exhibiting the metallic conduction. The revelation of highly dispersed Au^{+} ions was reported to be affected by channel dimensions and surface areas of the employed zeolite. These results are in agreement with those obtained from IR and DTA data.

References

[1] J.C. Dyre, T.B. Schroder, Rev. Modern Phys. 72 (3) (2000) 873.
[2] D.L. Sidebottom, Phys. Rev. Lett. 82 (1999) 3656.
[3] A.S.Md.S. Rahman, M.H. Islam, C.A. Hograth, Int. J. Electron. 62 (1987) 167.
[4] W. Wackawek, M. Kulesza, M. Zabkowska, Mater. Sci. 7 (1981) 385.
[5] A. Goswami, A.P. Goswami, Thin Solid Films 16 (1973) 175.
[6] S.I. Shihub, R.D. Gould, Phys. Status Solidi A 139 (1993) 129.
[7] C. Hamman, Phys. Status Solidi A 26 (1968) 311.
[8] S.R. Elliot, Philos. Mag. 36 (1977) 1291.
[9] G.E. Pike, Phys. Rev. B 6 (1972) 1572.
[10] M.M. Mohamed, T.M. Salama, R. Ohnishi, M. Ichikawa, Langmuir 17 (2001) 5678.
[11] M.M. Mohamed, M. Ichikawa, J. Colloid Interf. Sci. 232 (2000) 381.
[12] T.M. Salama, R. Ohnishi, M. Ichikawa, J. Chem. Soc., Faraday Trans. 92 (2) (1996) 301.
[13] M. Haurta, N. Yamada, T. Kobayashi, S. Iijima, J. Catal. 115 (1989) 301.
[14] H. Yoshida, K. Kimura, Y. Inaki, T. Hattori, J. Chem. Soc., Chem. Commun. (1997) 129.
[15] M. Ichikawa, Adv. Catal. 38 (1992) 284.
[16] S. Inagaki, Y. Fukushima, K. Kuroda, J. Chem. Soc., Chem. Commun. (1993) 680.
[17] J.S. Beck, J.C. Vartuli, W.J. Roth, M.E. Leonowicz, C.T. Kreage, K.D. Smitt, I.W. Chu, D.H. Olson, E.W. Sheppard, S.B. McCulleni, J.B. Higgins, J.L. Schlenker, J. Am. Chem. Soc. 114 (1992) 10834.
[18] T. Yamamoto, T. Shido, S. Inagaki, Y. Fukushima, M. Ichikawa, J. Am. Chem. Soc. 118 (1996) 5810.
[19] T.M. Salama, T. Shido, H. Mingawa, M. Ichikawa, J. Catal. 152 (1995) 322.
[20] T.M. Salama, T. Shido, R. Ohnishi, M. Ichikawa, J. Phys. Chem. 100 (1996) 3688.
[21] S. Summerfield, Philos. Mag. B 52 (1985) 9.
[22] M.B. Sayed, Microporous Mater. 6 (1996) 181.
[23] M.B. Sayed, Microporous Mesoporous Mater. 37 (2000) 107.